Laser alignment as a route to ultrafast control of electron transport through junctions

Matthew G. Reuter, Mark A. Ratner, and Tamar Seideman

Phys. Rev. A **86**, 013426 — Published 30 July 2012

DOI: 10.1103/PhysRevA.86.013426

Laser Alignment as a Route to Ultrafast Control of Electron Transport through Junctions

Matthew G. Reuter,[1,2] Mark A. Ratner,[1] and Tamar Seideman[1,*]

[1] *Department of Chemistry, Northwestern University, Evanston, Illinois 60208, USA*

[2] *Computer Science and Mathematics Division and Center for Nanophase Materials Sciences, Oak Ridge National Laboratory, Oak Ridge, Tennessee 37831, USA*

(Dated: July 9, 2012)

Abstract

We consider the extension of ultrafast laser alignment schemes to surface-adsorbed molecules, where the laser field coerces the molecule to reorient itself relative to the surface. When probed by a scanning tunneling microscope tip, this reorientation modifies the tip-molecule distance, and thus the tunneling current, suggesting a route to an ultrafast, nanoscale current switch. In addition to exploring the controllability of adsorbed molecules by moderately intense laser fields and discussing the fundamental differences of alignment behavior between surface-adsorbed molecules and gas phase molecules, we computationally investigate the quality of orientation with respect to field intensity, field duration, and the location of the tip. Overall, the molecule moves directly to its oriented configuration, which is reasonably insensitive to the tip location. These results collectively suggest the efficacy of using laser alignment schemes to control electron transport through junctions.

PACS numbers: 32.80.Qk, 34.35.+a, 82.37.Gk, 82.50.Nd

* t-seideman@northwestern.edu

I. INTRODUCTION

Nonadiabatic laser alignment—the application of laser pulses to coherently control the orientational properties of molecules—has evolved over the past 15 years from a theoretical dream [1] into a rich field of experimental and theoretical research with a growing number of applications [2–28]. For reviews, please see Refs. 6 and 10. In this approach, a moderately-intense (below off-resonance ionization thresholds), short (with respect to the rotational period of the molecule) laser pulse populates a rotationally-broad wavepacket. The phase relations among the rotational components guarantee that the molecule will, at a controllable delay, align after the pulse turn-off and subsequently exhibit a characteristic revival pattern. For the case of classically-stable motions in the isolated molecule limit (as in linear or symmetric top molecules), the alignment attained after the pulse turn-off is precisely reconstructed at multiples of the rotational period. Dissipative environments frustrate these alignment revivals [29, 30]; weak dissipation (such as in a dense gas) gradually diminishes the amplitudes of sequential revivals whereas strong dissipation (rapid compared to the system rotational periods) only allows the observation of alignment immediately following the laser pulse.

The majority of laser alignment studies to date have focused on the case of small molecules isolated in molecular beams. Given, however, the vast arena of potential applications for laser alignment in chemistry and materials sciences, we expect the focus of this research to shift to complex molecular systems, including ones subject to dissipative environments, in future years. As first steps toward this goal, various theoretical and experimental studies have reported on the extension of alignment concepts to molecules in dense, dissipative media [13, 16, 28–33], to ensembles of molecules [34–37], and to nonrigid polyatomic molecules, where torsional alignment can be established [38–44]. Recent applications of laser alignment schemes in complex media include the control of charge transfer, the separation of nuclear spin isomers, and the manipulation of molecular chirality [40–42, 45].

To the best of our knowledge, the first extension of the alignment concept to address materials science challenges is presented in Ref. 46, which proposes an ultrafast, nanoscale electric switch by applying nonadiabatic alignment to a surface-adsorbed molecule. In this approach, a long-chain organic molecule is adsorbed onto a silicon surface and is subjected to a scanning tunneling microscope (STM) tip. The alignment laser pulse reorients the

molecule within the junction, changing the tip-molecule distance and, thus, the tunneling current. Other approaches for using light to control electron transport through a junction are presented in Refs. 18, 47–53.

The design in Ref. 46 offers several attractive features of more general potential. The use of a semiconducting (rather than metallic) surface and low (sub-bandgap) frequencies circumvents the hurdle of substrate-mediated processes [54], which have hindered early schemes to coherently control electron transport through junctions with light. The sharp metal tip also serves to enhance the incident electric field, localizing the field below the tip apex [55–57], while doubling as a conducting electrode. Lastly, the substrate enhances the adsorbate polarizability as compared to the isolated molecule and hence also the strength of the field-matter interaction.

Our goal in the present work is to investigate the generality of using laser alignment schemes to manipulate the orientation of surface-adsorbed molecules. Previous work [46] demonstrated, as proof-of-concept, that such control over surface-adsorbed molecules is feasible under ideal circumstances, *i.e.*, using a linear molecule on an isotropic (atomically flat) surface with the STM tip directly above the site of adsorption. In establishing these general principles, a relatively simple molecule (an oligo-yne) was considered, which is chemically unstable [58]. Moreover, such an isotropic surface is an unverified approximation, and, to be technologically-relevant, the quality of alignment should be reasonably insensitive to the location of the STM tip. In the present work we thus revisit the alignment of surface-adsorbed molecules with a particular interest in these more general, "unideal" situations. To this end, we incorporate both surface anisotropy and STM tip location into our model, yielding a more detailed description of the adsorption chemistry and also allowing us to examine the interplay between the laser field and the metal tip. Finally, we propose and explore a molecule that would make a convenient candidate for the experimental realization of our control approach.

The layout of this paper is as follows. Section II describes our model, introduces our candidate system, and details the computational techniques used throughout. Then, in Sec. III we examine the role of field intensity, surface anisotropy, and STM tip location on the quality of alignment. We find that surface anisotropy is largely negligible for the laser pulses considered here and that the quality of alignment is reasonably robust with respect to STM tip location. These results support the validity of the conclusions in Ref. 46 while also

pointing to new control opportunities for both vibrational dynamics and electron transport in molecular junctions. Finally, we conclude and suggest future directions in Sec. IV.

II. THEORETICAL MODEL AND COMPUTATIONAL DETAILS

The envisioned setup is depicted schematically in Fig. 1(a). At the simplest level, our system consists of a STM tip and a conjugated, quasi-linear organic molecule adsorbed onto a doped silicon surface [46]. When compared to an isolated molecule, adsorption to the surface fundamentally changes some of the physics pertinent to laser alignment schemes. First, the molecule is subject to an adsorption potential and will preferentially rest at an equilibrium configuration in the absence of an electric field. We denote this configuration as ($\theta_{\rm eq}$, $\varphi_{\rm eq}$), where $0^\circ \leq \theta < 90^\circ$ is the polar angle (measured with respect to the surface normal) and $0^\circ \leq \varphi < 360^\circ$ is the azimuthal angle [following standard convention [59], measured with respect to the x-axis, here defined as the direction perpendicular to a silicon(100) dimer row]. Second, adsorption constrains the range of molecular motion. Instead of freely rotating, the adsorbed molecule librates around its equilibrium configuration, and, additionally, cannot penetrate the substrate (restricting $\theta < 90^\circ$). Consequently, the laser field not only aligns the molecule (as is the case for gas or solution phase systems), but also orients it. Finally, whereas alignment in the gas phase is determined by a competition between the laser-induced potential and thermal energy, on the surface the laser-induced potential competes with the adsorption potential. For this reason temperature will have only a minor effect on alignment [46] (in contrast with the gas phase case) throughout the range of relevance to low-temperature STM experiments (see, *e.g.*, Refs. 60 and 61).

Putting this all together, the total Hamiltonian for our system is,

$$\mathcal{H}(t) = \mathcal{T} + \mathcal{V}_{\rm ads} + \mathcal{V}_{\rm ind}(t), \tag{1}$$

where

$$\mathcal{T} = \frac{-\hbar^2}{2I_{\rm inertia}} \left[\frac{1}{\sin\theta} \frac{\partial}{\partial\theta} \left(\sin\theta \frac{\partial}{\partial\theta} \right) + \frac{1}{\sin^2\theta} \frac{\partial^2}{\partial\varphi^2} \right]$$

is the kinetic energy, $\mathcal{V}_{\rm ads}$ is the adsorption potential, $\mathcal{V}_{\rm ind}(t)$ is the laser-induced potential, and $I_{\rm inertia}$ is the molecular moment of inertia. The remainder of this section is devoted to the theoretical and computational details for (i) obtaining the field-free and field-induced potentials and (ii) simulating the dynamical motion of surface-adsorbed molecules in response

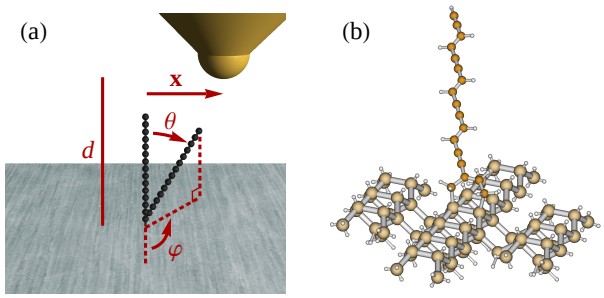

FIG. 1. (Color online) (a) Schematic of the STM tip, molecule, and surface, defining (i) the polar angle of the molecule with respect to the surface normal, θ; (ii) the azimuthal angle of the molecule, φ; (iii) the height of the STM tip above the surface, d; and (iv) the lateral displacement of the STM tip from the site of adsorption, $\mathbf{x}$. (b) The system numerically investigated in this work, an oligo-diacetylene, attached to a silicon cluster.

to laser irradiation.

A. Adsorption Potential

Our transport control approach is based on the rapid orientation of the adsorbed molecule with the surface normal, switching the system from the equilibrium, nonconducting configuration, to the oriented, conducting configuration. The approach is thus applicable to any molecule that adsorbs at an angle different from the surface normal, provided that the laser-induced potential is sufficiently large to surpass the field-free adsorption potential. Note that both the intensity enhancement by the tip and the polarizability enhancement by the substrate serve to increase the laser-induced potential. As a concrete example, we consider an oligo-diacetlyene molecule (with, formally, a single-triple-single-double bond alternation pattern) adsorbed to a Si(100) surface via a butadiene linking group. A rendering of this molecule on a silicon cluster is shown in Fig. 1(b). This oligo-diacetylene repeat unit is more stable [58, 62] than the oligo-yne unit used previously [46], and the butadiene linker was chosen based on chemisorption studies of organic molecules with Si(100) surfaces [63, 64].

We calculate the adsorption potential with a cluster model of a hydrogen-passivated Si(100)-2×1 surface [46, 65]. To verify convergence with respect to cluster size, clusters of both 17 and 75 silicon atoms were used, and the adsorption potentials were comparable for the two systems [66]. The large and small clusters are depicted in Figs. 1(b) and 2, respec-

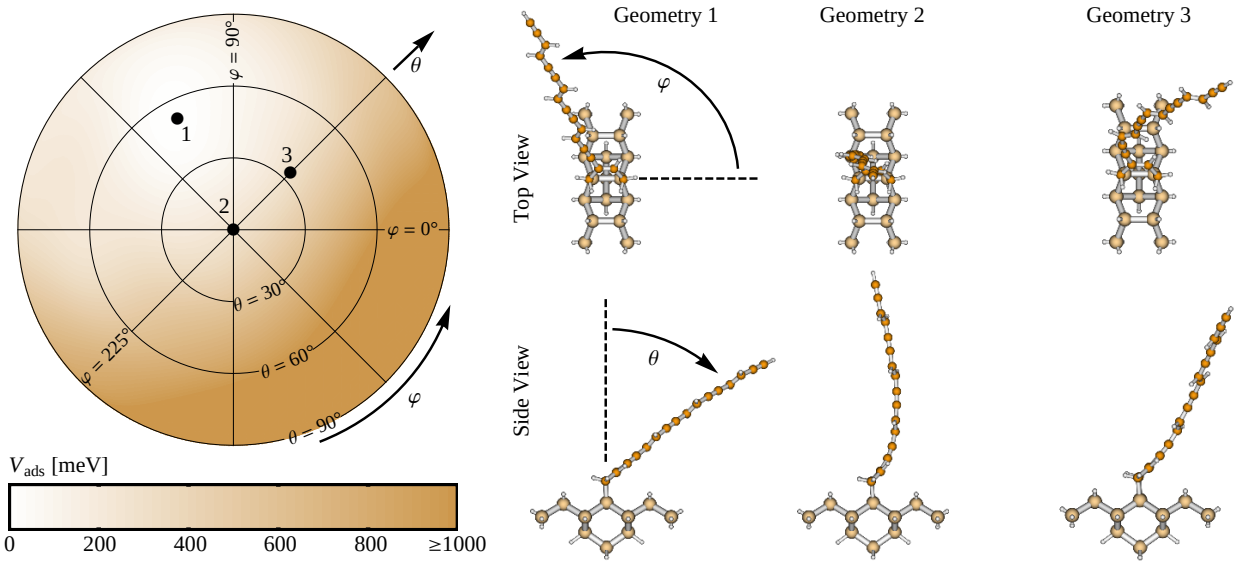

FIG. 2. (Color online) (Left) Adsorption potential, $\mathcal{V}_{\text{ads}}$, as a function of the polar and azimuthal angles defined in Fig. 1. In this and subsequent figures, the angular parameter space is plotted in 2D polar coordinates with the polar angle (θ) depicted radially. (Right) Several molecular configurations, as marked in the left plot. Geometry 1 is the field-free equilibrium configuration and geometry 2 is the upright configuration (with $\theta = 0°$).

tively. At each angular point, the adsorption potential was computed with Q-Chem [67] using the B3LYP functional of the density functional theory and the 6-31G basis set. Figure 2 displays the adsorption potential for our oligo-diacetylene along with several configurations, including the equilibrium configuration ($\theta_{\text{eq}} = 53°$, $\varphi_{\text{eq}} = 117°$). Note that, since the azimuthal angle becomes degenerate as $\theta \to 0°$ [see Fig. 1(a)], we use 2D polar coordinates with θ as the radial variable to plot quantities in the (θ, φ) angle space.

B. Laser-Induced Potential

In this work we consider laser pulses that are linearly polarized parallel to the tip axis and tuned to a low frequency, below the substrate bandgap (*ca.* 1 eV for silicon) [68]. Applied to the junction, the field is plasmon-enhanced and strongly localized below the tip apex, which distorts its linear polarization near the apex. At the far-off-resonant frequencies considered, the tip-enhanced field interacts predominantly with the molecular polarizability tensor (as

modified by the surface); hence, the laser-induced potential has the form [10]

$$\mathcal{V}_{\mathrm{ind}}(t) = -\frac{1}{4}\vec{\varepsilon}(t; d, \mathbf{x}) \cdot \alpha(\theta, \varphi)\vec{\varepsilon}(t; d, \mathbf{x}). \tag{2}$$

In Eq. (2), d is the height of the STM tip above the surface [see Fig. 1(a)], $\mathbf{x}$ is the lateral displacement of the tip from the site of adsorption, α is the space-fixed molecular polarizability tensor, and $\vec{\epsilon}(t; d, \mathbf{x}) = \vec{\varepsilon}(t; d, \mathbf{x}) \exp(-i\omega t) + \text{c.c.}$ is the plasmon-enhanced electric field vector. Furthermore, we consider steady-state electromagnetic field distributions since the optical frequencies of interest are below the silicon band gap; thus,

$$\vec{\varepsilon}(t; d, \mathbf{x}) = \varepsilon(t)\vec{s}(d, \mathbf{x}), \tag{3}$$

where $\varepsilon(t)$ is the laser pulse envelope and $\vec{s}$ is a dimensionless enhancement factor that accounts for both plasmon-enhancement of the electric field and any deviation from linear polarization near the tip apex ($\vec{s}$ is parallel to the field polarization vector directly under or far from the tip). Combining Eqs. (2) and (3), and recognizing that $I(t) = \varepsilon(t)^2$ is the intensity of the incident (far from the tip) laser field, we find that

$$\mathcal{V}_{\mathrm{ind}}(t) = -\frac{1}{4}I(t)\vec{s}(d, \mathbf{x}) \cdot \alpha(\theta, \varphi)\vec{s}(d, \mathbf{x}). \tag{4}$$

We proceed to discuss the numerical procedures for obtaining α and $\vec{s}$.

The polarizability tensor in the space-fixed frame is calculated in GAMESS [69] with the coupled-perturbed Hartree-Fock (CPHF) theory and the 6-31G** basis set. The oligodiacetylene/17-silicon atom cluster is used in these computations. We remark that, although all molecules are polarizable, their polarizability anisotropies vary significantly, roughly mirroring their geometric anisotropies.

In our previous work [46], $\vec{s}$ was calculated using three-dimensional finite-difference time-domain (FDTD) simulations [70]; however, practical computational issues limited the tip-surface distance to $d \geq 10$ nm. For most relevant configurations, the molecule is only 2–3 nm long, and these tip-surface distances are notably large. In this work, we instead use the multiresolution methods in the MADNESS (multiresolution adaptive numerical environment for scientific simulation) package [71] to calculate $\vec{s}$ for d down to 5 nm, where the standard technique for computing plasmonic enhancements—classical electromagnetism—encounters difficulties [72]. This algorithm is detailed in Ref. 73. Very briefly, $\vec{s}$ is obtained from an electrostatics calculation with an applied bias between a paraboloidal tip and the surface;

the enhancement factor is the resulting electric field normalized to the linear-polarized field far from the tip. Our MADNESS simulations agreed with our previous quasi-static FDTD results for $d = 10$ nm.

C. Quantum Dynamics

The dynamics of a surface-adsorbed molecule, as a dissipative system, is generally described by a density matrix formalism [74]. In the context of laser alignment, the phase relations established by the coherent laser pulse will eventually dissipate due to interactions with the substrate, returning the molecule to its equilibrium configuration. However, we expect dissipation to be slow compared to laser alignment since (i) alignment/orientation is quickly realized after the pulse turn-off (*vide infra*) and (ii) the butadiene linker group "insulates" the librating oligo-diacetylene chain from the surface. Therefore, during the time interval of relevance, the system can be approximated as non-dissipative, where the dynamics are governed by the time-dependent Schrödinger equation,

$$i\hbar \frac{\mathrm{d}\,|\Psi(t)\rangle}{\mathrm{d}t} = (\mathcal{T} + \mathcal{V}_{\mathrm{ads}} + \mathcal{V}_{\mathrm{ind}}(t))\,|\Psi(t)\rangle\,. \tag{5}$$

Since temperature plays a minor role in this system, we take the initial state to be the ground librational state, $|\Psi(t_0)\rangle = |\chi_0\rangle$, where

$$(\mathcal{T} + \mathcal{V}_{\mathrm{ads}})\,|\chi_j\rangle = E_j\,|\chi_j\rangle\,, \quad j = 0, 1, \ldots, \tag{6}$$

and $E_j \leq E_{j+1}$.

The dynamics are calculated using a recently developed extension of the second-order split-operator propagator [75–77],

$$|\Psi(t + \Delta t)\rangle = e^{-i\mathcal{T}\Delta t/(2\hbar)} e^{-i[\mathcal{V}_{\mathrm{ads}} + \mathcal{V}_{\mathrm{ind}}(t+\Delta t/2)]\Delta t/\hbar} e^{-i\mathcal{T}\Delta t/(2\hbar)}\,|\Psi(t)\rangle\,, \tag{7}$$

adapted to angular spaces [77, 78]. Owing to the rotational (librational) nature of our system, $\mathcal{T}$ is local in the angular momentum representation, whereas $\mathcal{V}_{\mathrm{ads}}$ and $\mathcal{V}_{\mathrm{ind}}$ are local in the $(\theta,\, \varphi)$ angle representation. Thus, the outer terms in Eq. (7) are most readily evaluated when $|\Psi(t)\rangle$ is expanded in the spherical harmonics [79], $\{Y_{\ell,m}\}$,

$$\langle \theta, \varphi\,|\,\Psi(t)\rangle = \Psi(\theta, \varphi, t) = \sum_{\ell=0}^{\infty} \sum_{m=-\ell}^{\ell} \Psi_{\ell,m}(t) Y_{\ell,m}(\theta, \varphi). \tag{8}$$

A fast spherical harmonic transform [80, 81] is used to convert between angle and angular momentum representations [78]. In the calculations that follow, $0.005 \leq \Delta t \leq 0.05$ fs (adaptive time stepping was used, allowing smaller time steps when the field intensity was high and larger time steps when the intensity was low) and the series in Eq. (8) is truncated at $\ell < 512$. (Laser pulses with lower intensities were run with the series truncated at $\ell < 400$. Convergence with respect to this truncation threshold was confirmed by monitoring the wavefunction norm.) Due to the restriction that $\theta < 90°$, we only use the spherical harmonics with $\ell + m$ odd, since these spherical harmonics vanish at $\theta = 90°$. Finally, the ground state of a time-independent Hamiltonian [*e.g.*, Eq. (6) for the librational states] is obtained using imaginary time propagation [82] with $\ell < 128$.

III. COHERENT, NONADIABATIC ORIENTATION IN THE STM JUNCTION

With the Hamiltonian defined, we proceed to examine the robustness of the orientation behavior with respect to, in particular, the location of the STM tip. First, in Sec. III A, we discuss the notion of the oriented configuration and consider how the tip location may affect it. Then, Secs. III B and III C explore the roles of the incident field intensity and the laser pulse envelope, respectively, on the quality of orientation. Finally, Sec. III D discusses the interplay between the laser intensity, the tip location, and the plasmon-modified polarization in determining the orientation dynamics.

A. The "Oriented" Configuration

Regarding laser alignment as a general tool for manipulating the orientation and configuration of the surface-adsorbed molecule, we have that the desired behavior, and thus the target configuration, depends on the context and goals of the envisioned application. The specific study of Ref. 46, for instance, sought an ultrafast switch for electric current. Laser alignment coerced the molecule to arise from its equilibrium configuration, thereby reducing the vacuum tunneling distance between the tip and the molecule and thus increasing the current. Since the tip was assumed to be directly above the site of adsorption ($\mathbf{x} = \mathbf{0}$), the sought configuration was $\theta = 0°$.

A closely related, but more general question is how far a moderately intense (noninvasive)

laser field can drive the adsorbed molecule from its equilibrium configuration. In other words, to what configuration will the molecule reorient as the laser pulse becomes increasingly intense? This optimally-"oriented" configuration, denoted ($\theta_{\rm opt}$, $\varphi_{\rm opt}$), is analogous to the equilibrium configuration in that ($\theta_{\rm opt}$, $\varphi_{\rm opt}$) minimizes $\mathcal{V}_{\rm ind}$ whereas ($\theta_{\rm eq}$, $\varphi_{\rm eq}$) minimizes $\mathcal{V}_{\rm ads}$. Figure 3 displays $\theta_{\rm opt}$ for the oligo-diacetylene molecule as a function of the tip location. As expected, the tip only impacts $\theta_{\rm opt}$ when near the site of adsorption, here $|\mathbf{x}| \lesssim 25$ nm, and, accordingly, the effects of tip location are more pronounced when d is smaller.

Consider next the variations in $\theta_{\rm opt}$ and first suppose that the tip is far from the site of adsorption. Then, the field is linearly-polarized near the molecule, and $\theta_{\rm opt} \approx 8^\circ$ (not 0°) since the butadiene linking group slightly shifts the oligo-diacetylene chain (see Fig. 2). As the tip moves closer to the molecule, the molecule responds to the tip-enhanced field by pointing at the tip (where the enhancement is strongest). Should the tip approach the molecule from the right (relative to the side views in Fig. 2), this propensity to point at the tip essentially depresses the molecule, and $\theta_{\rm opt}$ increases to $\sim 20^\circ$ at $d = 5$ nm. As the tip then moves closer to the site of adsorption, the field becomes more linearly-polarized (and also more intense), and $\theta_{\rm opt}$ returns to 8°. Finally, the molecule continues to follow the tip as the tip moves beyond the site of adsorption; $\theta_{\rm opt}$ passes through 0°, and even starts increasing (along a different $\varphi_{\rm opt}$ azimuth) before eventually returning to the linear-polarized $\theta_{\rm opt}$ when the tip is again sufficiently far away. The various stages of this path are illustrated in Fig. 3.

B. Field Intensity

As discussed above, the tip location greatly affects $\mathcal{V}_{\rm ind}$ when the tip is near the molecule, here for $|\mathbf{x}| \lesssim 25$ nm and $d \lesssim 10$ nm. Orientation, however, is determined by the balance of $\mathcal{V}_{\rm ads}$ and $\mathcal{V}_{\rm ind}$. We thus proceed to explore the intensity dependence of molecular orientation, and, to that end, display the complete potential, $\mathcal{V}_{\rm ads} + \mathcal{V}_{\rm ind}$, for various tip locations and intensities in Fig. 4. Unsurprisingly, the potential energy well moves from the equilibrium to the oriented configuration as the intensity increases, and the laser-induced potential well depth increases when d decreases.

Transitioning to explore the quality of orientation, we first consider the case of a long laser pulse (with respect to the librational period, $\sim$2 ps) that adiabatically switches the

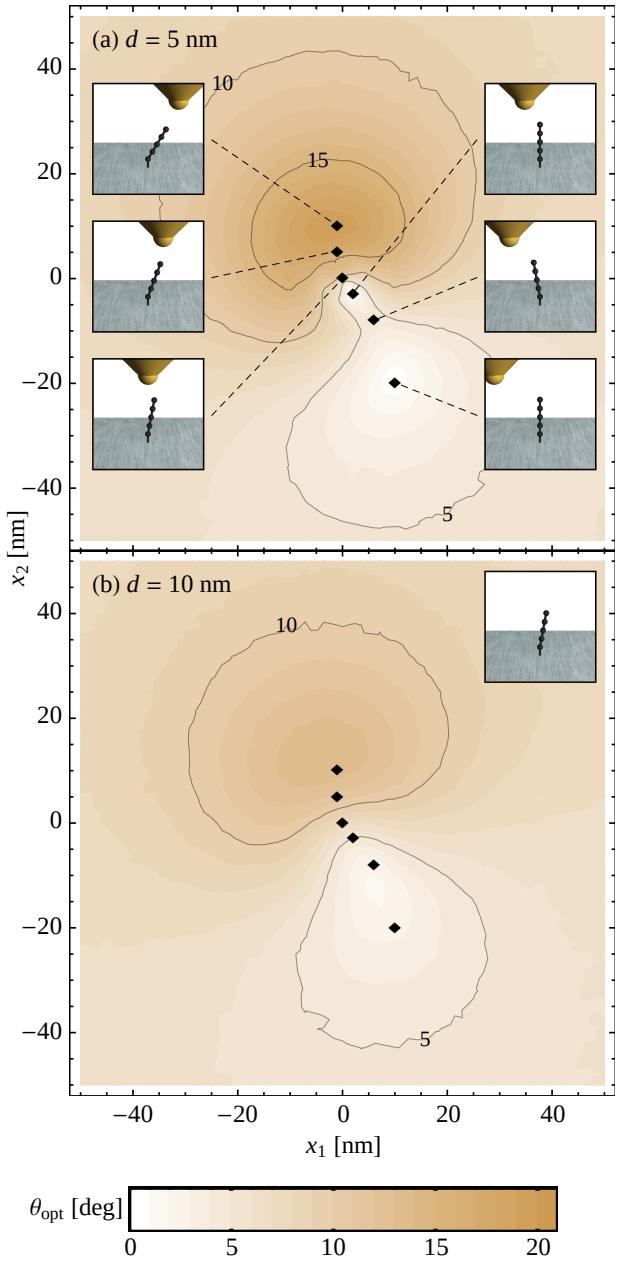

FIG. 3. (Color online) $\theta_{\rm opt}$, the polar angle that minimizes $\mathcal{V}_{\rm ind}$, as a function of the tip location [$\mathbf{x} = (x_1, x_2)$ is the lateral displacement from the site of adsorption and d is the height of the tip above the surface]. When the tip is far from the oligo-diacetylene molecule (illustratively, the bottom-most inset), $\theta_{\rm opt} \approx 8^\circ$. As the tip approaches the site of adsorption, the molecule attempts to point at the tip since the tip-enhanced electric field is strongest directly under the tip apex. Due to the asymmetry of the butadiene linking group, $\theta_{\rm opt}$ may increase in some directions (left-most insets), while decreasing in others (top-right insets). The shape of $\mathcal{V}_{\rm ind}$ is strongly dependent on the tip location when the tip is sufficiently close to the molecule.

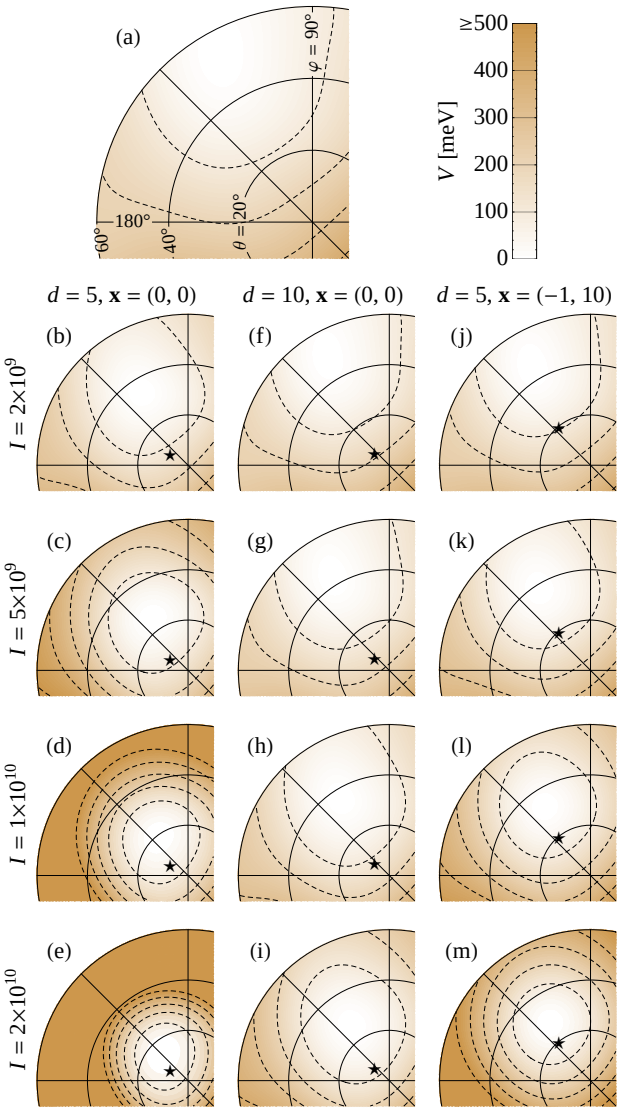

FIG. 4. (Color online) The complete potential, $\mathcal{V}_{\rm ads} + \mathcal{V}_{\rm ind}$, for various tip locations and intensities. The tip location variables, d and $\mathbf{x}$, are given in nm and the field intensity, I, is in W cm^{-2}. The (field-free) adsorption potential is displayed in panel (a). As the intensity increases, the potential energy well moves toward the oriented configuration (see Fig. 3), which is starred in each of the panels (b)–(h). For reference, contours of $V = 100$, 200, 300, 400, and 500 meV are also displayed in each panel (dashed lines).

molecule into and out of orientation. The degree of orientation is quantified in Fig. 5 via the expectation value of θ, where $\langle\theta\rangle = 0°$ corresponds to an upright molecule. As the intensity increases, the molecule gradually reorients to its oriented configuration, reaching, in most cases, that orientation for $I \gtrsim 10^{11}$ W cm^{-2}. The rapid increase of orientation with

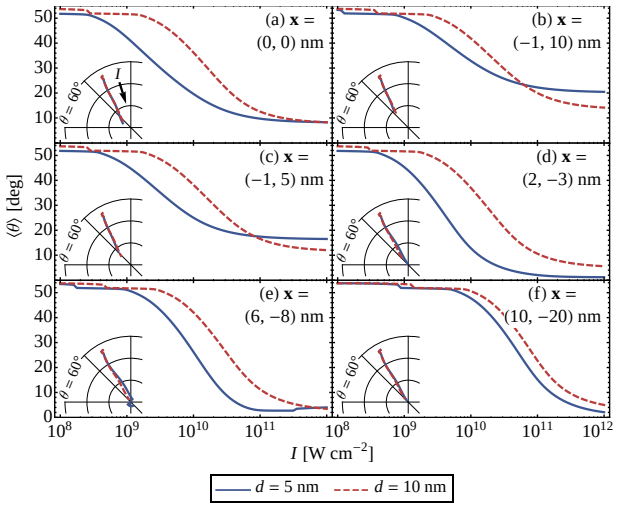

FIG. 5. (Color online) Averaged orientation vs. incident intensity for adiabatic excitation when the STM tip is at the six locations marked in Fig. 3. As expected from Fig. 4, the molecule moves toward its oriented configuration as the intensity increases, and, for most tip locations, $I \approx 10^{11}$ W cm^{-2} is sufficient to orient the molecule. The insets show that the azimuthal angle remains largely constant as the molecule approaches its oriented configuration.

the intensity about $I \approx 10^{10}$ W cm^{-2} indicates the intensity range where the laser-induced potential nears and exceeds the adsorption potential barrier at $\theta_{\rm opt}$, see Fig. 4.

Besides showing that the tip-enhanced fields in the current setup induce alignment at much lower intensities than those typically required in gas phase experiments [6], Fig. 5 also reveals that the azimuthal angle is reasonably constant as the molecule moves to the oriented configuration. In this sense we validate the isotropic surface approximation (neglect of φ) employed in the previous work [46]; the molecule moves directly from the equilibrium to the oriented configuration. Regarding the location of the tip, it is interesting to note that, in Figs. 5(b) and (c), moving the tip away from the surface counterintuitively drives the molecule further from $\theta_{\rm eq}$ at sufficient intensities. Quite simply, the tip holds the molecule down at these locations (see Fig. 3), and increasing d diminishes this effect by restoring a more linearly-polarized electric field near the molecule.

C. Laser Pulse Envelope

Having established the possibility of sharply orienting the molecule at moderate laser intensities, we proceed to investigate the quality and timescale of nonadiabatic alignment (orientation). We consider laser pulses with Gaussian envelopes,

$$I(t) = I_{\max} \exp\left[-\frac{t^2}{2\sigma^2}\right], \tag{9}$$

where $I_{\max}$ is the maximum pulse intensity and σ determines the pulse duration. Although interesting physics arises when σ for the pulse turn-on and turn-off are different (*e.g.*, the case of adiabatic turn-on followed by rapid turn-off of the laser pulse [6, 10]), for simplicity we only consider here the case of a symmetric pulse.

Figure 6 displays $\langle\theta\rangle$ and I as functions of time under nonadiabatic conditions. The pulses denoted by dashed green and solid blue lines in Fig. 6 have a common peak intensity ($I_{\max}$), whereas the dot-dashed red and solid blue pulses share the same fluence. The orientation in response to these pulses exhibits several of the general features of nonadiabatic alignment (orientation). Notably, the orientation falls from its equilibrium configuration near 53° after the pulse turns off and reaches a minimum, $\langle\theta\rangle_{\min}$, in the field-free domain. Increasing the pulse duration (provided it remains short as compared to the librational period) with constant peak intensity drives the molecule closer to its oriented configuration; as evidenced in Fig. 6, the degree of orientation is determined by the fluence of the pulse [46]. Thus, lengthening or intensifying the pulse will enhance the degree of orientation in a similar fashion. As a computational aside, pulses with higher fluences require smaller time steps and larger basis sets (a higher cutoff for ℓ); the pulses considered here exemplify the general physical behavior we expect without incurring undue computational expense.

D. Interplay between the Tip and Laser Polarization

Having addressed the notion of an oriented configuration and the roles of intensity and pulse envelope on the degree of alignment, we finally investigate the effects of the STM tip location on the quality of orientation. We quantify the quality of orientation through

$$\eta \equiv \frac{\theta_{\rm eq} - \langle\theta\rangle_{\min}}{\theta_{\rm eq} - \theta_{\rm opt}}, \tag{10}$$

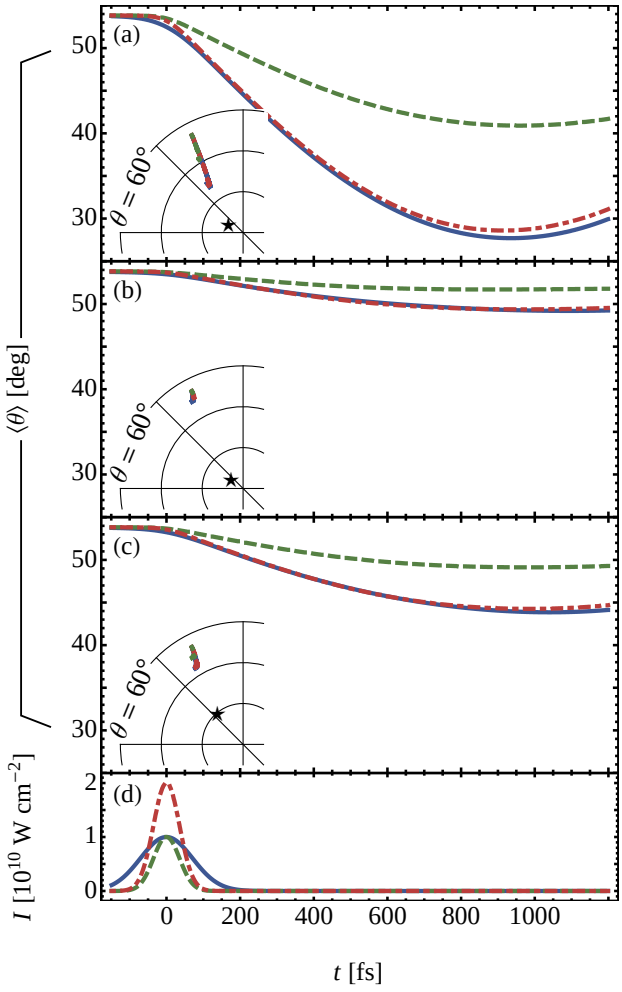

FIG. 6. (Color online) Averaged orientation in the nonadiabatic domain: $\langle\theta\rangle$ vs. intensity and pulse duration. The incident laser pulse intensities, $I(t)$, are shown in panel (d); dot-dashed red line: $I_{\max} = 2 \times 10^{10}$ W cm^{-2}, $\sigma = 50$ fs; dashed green line: $I_{\max} = 1 \times 10^{10}$ W cm^{-2}, $\sigma = 50$ fs; solid blue line: $I_{\max} = 1 \times 10^{10}$ W cm^{-2}, $\sigma = 100$ fs. The other panels show the orientation for the tip at (a) $d = 5$ nm, $\mathbf{x} = (0, 0)$ nm; (b) $d = 10$ nm, $\mathbf{x} = (0, 0)$ nm; (c) $d = 5$ nm, $\mathbf{x} = (-1, 10)$ nm. The insets show the molecular trajectory relative to the oriented configuration. Provided the pulse is sufficiently short, the pulse fluence fully determines the degree of orientation.

where $\langle\theta\rangle_{\min}$ is the minimum $\langle\theta\rangle$ experienced by the molecule in response to the pulse; $\eta = 1$ indicates the molecule reaches its oriented configuration. Figure 7 shows that, for a given pulse (here $I_{\max} = 1 \times 10^{10}$ W cm^{-2} and $\sigma = 100$ fs), the degree of orientation is fairly constant when the tip is within several nanometers of the site of adsorption. The orientation quality shows a similar trend; the STM tip can be several nm from the site of adsorption

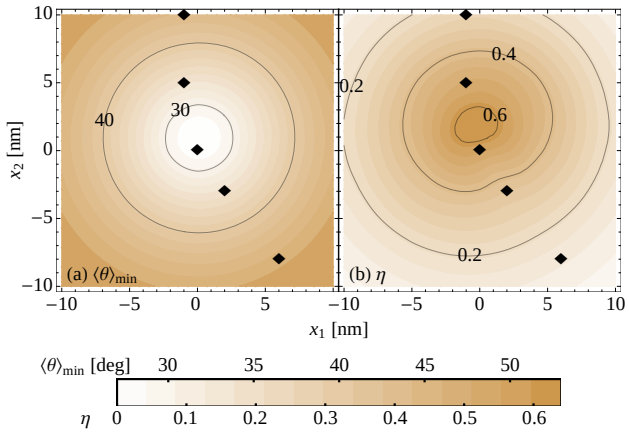

FIG. 7. (Color online) (a) The degree of orientation, $\langle\theta\rangle_{\rm min}$, and (b) the quality of orientation, η, obtained for various tip locations, $\mathbf{x} = (x_1, x_2)$ and $d = 5$ nm. Similar effects, although much more muted, are observed for $d = 10$ nm. The solid blue pulse from Fig. 6, $I_{\rm max} = 1 \times 10^{10}$ W cm^{-2} and $\sigma = 100$ fs, is considered here; a pulse with greater fluence would enhance $\langle\theta\rangle_{\rm min}$ and η. Both the degree and quality of orientation are stable to small changes in the tip location from the site of adsorption, $|\mathbf{x}| \lesssim 3$ nm in this case, indicating the robustness of applying laser alignment schemes to surface-adsorbed molecules. For reference, the tip locations marked in Fig. 3 are also marked here.

and still allow moderately-intense laser pulses to drive a surface-adsorbed molecule away from its field-free equilibrium configuration. Our results suggest not only the applicability of strong laser control methods to adsorbed systems, but also (i) the robustness of laser alignment (orientation) in the STM junction with respect to the tip location and (ii) the enhanced controllability of such systems that arises from both the combination of their enhanced polarizability and the intensity enhancements in plasmonic environments.

IV. CONCLUSIONS

In the previous section, we examined the viability of using laser alignment concepts to manipulate the orientation of surface-adsorbed molecules. The use of a STM tip in our setup allows orientation to occur at significantly lower laser intensities than in gas phase systems and also introduces the location of the tip as a control variable. As we have shown, the tip location does not perturb the degree or quality of molecular orientation when the tip is

sufficiently close to the site of adsorption (perhaps $|\mathbf{x}| \lesssim 3$ nm), but it modifies the local polarization of the field, hence tuning the orientation in the nanoscale. Thus, alignment approaches introduce not only new applications but also new physical phenomena when applied to surface-adsorbed molecules.

Additionally, we were able to validate the "isotropic surface" approximation used previously [46] by performing higher-dimensional quantum calculations of the molecule/surface potential energy and polarizability surfaces and then exploring the laser-controlled reaction subject to these surfaces. We found that the molecule takes a direct path from its field-free equilibrium configuration to its oriented configuration; the dynamics are essentially independent of the azimuthal angle. From a computational perspective, neglecting the azimuthal angle significantly reduces the basis set size, thereby facilitating the study of surface-adsorbed molecules with more interesting internal structure. For instance, our approach might be extended to simultaneously control torsional and librational motion [41, 48]. Finally, we introduced a molecular system that we trust would make a convenient candidate for experimental realization.

Our study carries interesting implications to, and possible applications in, several areas. One is molecular nanoplasmonics—the combination of molecules with nanoparticles in hybrid constructs—where strong fields and strong spatial and orientational field gradients are naturally found [36]. Here, our results point to opportunities for the present and other strong-field control approaches to introduce new physical phenomena and assist the development of nanoscale materials with desired properties. Another is the growth of ordered molecular films [83], where the alignment field induces long range translational and orientational order and may give rise to preferred film morphologies and functionalities [34]. Third, and of specific interest, is control of electron transport through molecular junctions. Here, a moderately intense laser field can be used to rapidly switch the molecule into and out of a conducting configuration [46, 48], and can possibly lead to negative differential resistance [84]. Finally, controlled optical irradiation of molecular-scale junctions introduces new fundamental questions [18, 85], and, with recent advanced technologies [86], is currently becoming experimentally realizable.

ACKNOWLEDGMENTS

We are grateful to Maxim Sukharev and Robert Harrison for helpful conversations and to the Department of Energy (Grant numbers DE-FG02-04ER15612, DE-SC0001785) and the National Science Foundation (Grant number CHE-1012207/001) for support. M.G.R. performed this research as a Department of Energy Computational Science Graduate Fellow (Grant No. DE-FG02-97ER25308) while at Northwestern University and as a Eugene P. Wigner Fellow at the Oak Ridge National Laboratory, which is managed by UT-Battelle, LLC, for the Department of Energy under Contract DE-AC05-00OR22725. Some of the numerical work reported here employed resources of the Oak Ridge Leadership Computing Facility at the Oak Ridge National Laboratory.

---

[1] T. Seideman, J. Chem. Phys. **103**, 7887 (1995).

[2] W. S. Warren, H. Rabitz, and M. Dahleh, Science **259**, 1581 (1993).

[3] F. Rosca-Pruna and M. J. J. Vrakking, Phys. Rev. Lett. **87**, 153902 (2001).

[4] H. Rabitz, Science **299**, 525 (2003).

[5] M. Leibscher, I. S. Averbukh, and H. Rabitz, Phys. Rev. Lett. **90**, 213001 (2003).

[6] H. Stapelfeldt and T. Seideman, Rev. Mod. Phys. **75**, 543 (2003).

[7] M. Leibscher, I. S. Averbukh, and H. Rabitz, Phys. Rev. A **69**, 013402 (2004).

[8] J. Itatani, J. Levesque, D. Zeidler, H. Niikura, H. Pépin, J. C. Kieffer, P. B. Corkum, and D. M. Villeneuve, Nature **432**, 867 (2004).

[9] T. Kanai, S. Minemoto, and H. Sakai, Nature **435**, 470 (2005).

[10] T. Seideman and E. Hamilton, Adv. At. Mol. Opt. Phys. **52**, 289 (2006).

[11] V. Kumarappan, S. S. Viftrup, L. Holmegaard, C. Z. Bisgaard, and H. Stapelfeldt, Phys. Scr. **76**, C63 (2007).

[12] A. Goban, S. Minemoto, and H. Sakai, Phys. Rev. Lett. **101**, 013001 (2008).

[13] T. Vieillard, F. Chaussard, D. Sugny, B. Lavorel, and O. Faucher, J. Raman Spectrosc. **39**, 694 (2008).

[14] C. Z. Bisgaard, O. J. Clarkin, G. Wu, A. M. D. Lee, O. Geßner, C. C. Hayden, and A. Stolow, Science **323**, 1464 (2009).

[15] O. Ghafur, A. Rouzée, A. Gijsbertsen, W. K. Siu, S. Stolte, and M. J. J. Vrakking, Nature Phys. **5**, 289 (2009).

[16] D. Zhdanov and H. Rabitz, Phys. Rev. A **83**, 061402(R) (2011).

[17] C. Vallance, Phys. Chem. Chem. Phys. **13**, 14427 (2011).

[18] L. Wang and V. May, Phys. Chem. Chem. Phys. **13**, 8755 (2011).

[19] S. Zhang, C. Lu, T. Jia, Z. Wang, and Z. Sun, Phys. Rev. A **83**, 043410 (2011).

[20] S. Zhdanovich, A. A. Milner, C. Bloomquist, J. Floß, I. S. Averbukh, J. W. Hepburn, and V. Milner, Phys. Rev. Lett. **107**, 243004 (2011).

[21] S. Zhang, C. Lu, T. Jia, Z. Sun, and J. Qiu, J. Chem. Phys. **135**, 224308 (2011).

[22] X. Ren, V. Makhija, and V. Kumarappan, Phys. Rev. A **85**, 033405 (2012).

[23] J. P. Cryan, J. M. Glownia, J. Andreasson, A. Belkacem, N. Berrah, C. I. Blaga, C. Bostedt, J. Bozek, N. A. Cherepkov, L. F. DiMauro, L. Fang, O. Gessner, M. Gühr, J. Hajdu, M. P. Hertlein, M. Hoener, O. Kornilov, J. P. Marangos, A. M. March, B. K. McFarland, H. Merdji, M. Messerschmidt, V. S. Petrović, C. Raman, D. Ray, D. A. Reis, S. K. Semenov, M. Trigo, J. L. White, W. White, L. Young, P. H. Bucksbaum, and R. N. Coffee, J. Phys. B: At. Mol. Opt. Phys. **45**, 055601 (2012).

[24] V. Makhija, X. Ren, and V. Kumarappan, Phys. Rev. A **85**, 033425 (2012).

[25] J. P. Palastro, T. M. Antonsen Jr, S. Varma, Y.-H. Chen, and H. M. Milchberg, Phys. Rev. A **85**, 043843 (2012).

[26] R. Tehini, M. Z. Hoque, O. Faucher, and D. Sugny, Phys. Rev. A **85**, 043423 (2012).

[27] J. Yu, W. Zhang, J. Yang, and S.-L. Cong, Chem. Phys. **400**, 93 (2012).

[28] J.-M. Hartmann and C. Boulet, J. Chem. Phys. **136**, 184302 (2012).

[29] S. Ramakrishna and T. Seideman, Phys. Rev. Lett. **95**, 113001 (2005).

[30] S. Ramakrishna and T. Seideman, J. Chem. Phys. **124**, 034101 (2006).

[31] A. Pelzer, S. Ramakrishna, and T. Seideman, J. Chem. Phys. **126**, 034503 (2007).

[32] A. Pelzer, S. Ramakrishna, and T. Seideman, J. Chem. Phys. **129**, 134301 (2008).

[33] M. Artamonov and T. Seideman, **Submitted**.

[34] I. Nevo, S. Kapishnikov, A. Birman, M. Dong, S. R. Cohen, K. Kjaer, F. Besenbacher, H. Stapelfeldt, T. Seideman, and L. Leiserowitz, J. Chem. Phys. **130**, 144704 (2009).

[35] A. Birman, K. Kjaer, Y. Prior, I. Nevo, and L. Leiserowitz, Angew. Chem. Int. Ed. **49**, 2354 (2010).

[36] M. Artamonov and T. Seideman, Nano Lett. **10**, 4908 (2010).

[37] M. Artamonov and T. Seideman, Mol. Phys. **110**, 885 (2012).

[38] S. Ramakrishna and T. Seideman, Phys. Rev. Lett. **99**, 103001 (2007).

[39] C. B. Madsen, L. B. Madsen, S. S. Viftrup, M. P. Johansson, T. B. Poulsen, L. Holmegaard, V. Kumarappan, K. A. Jørgensen, and H. Stapelfeldt, Phys. Rev. Lett. **102**, 073007 (2009).

[40] C. B. Madsen, L. B. Madsen, S. S. Viftrup, M. P. Johansson, T. B. Poulsen, L. Holmegaard, V. Kumarappan, K. A. Jørgensen, and H. Stapelfeldt, J. Chem. Phys. **130**, 234310 (2009).

[41] S. M. Parker, M. A. Ratner, and T. Seideman, J. Chem. Phys. **135**, 224301 (2011).

[42] J. L. Hansen, J. H. Nielsen, C. B. Madsen, A. T. Lindhardt, M. P. Johansson, T. Skrydstrup, L. B. Madsen, and H. Stapelfeldt, J. Chem. Phys. **136**, 204310 (2012).

[43] S. M. Parker, M. A. Ratner, and T. Seideman, Mol. Phys. DOI:10.1080/00268976.2012.695808 (2012).

[44] B. Ashwell, S. Ramakrishna, and T. Seideman, **Submitted**.

[45] J. Floß, T. Grohmann, M. Leibscher, and T. Seideman, J. Chem. Phys. **136**, 084309 (2012).

[46] M. G. Reuter, M. Sukharev, and T. Seideman, Phys. Rev. Lett. **101**, 208303 (2008).

[47] J. Li, G. Speyer, and O. F. Sankey, Phys. Rev. Lett. **93**, 248302 (2004).

[48] I. Cacelli, A. Ferretti, M. Girlanda, and M. Macucci, Chem. Phys. **320**, 84 (2006).

[49] J. M. Mativetsky, G. Pace, M. Elbing, M. A. Rampi, M. Mayor, and P. Samorì, J. Am. Chem. Soc. **130**, 9192 (2008).

[50] L. Wang and V. May, J. Phys. Chem. C **114**, 4179 (2010).

[51] M. Sukharev and M. Galperin, Phys. Rev. B **81**, 165307 (2010).

[52] B. D. Fainberg, M. Sukharev, T.-H. Park, and M. Galperin, Phys. Rev. B **83**, 205425 (2011).

[53] U. Peskin and M. Galperin, J. Chem. Phys. **136**, 044107 (2012).

[54] J. W. Gadzuk, Surf. Sci. **342**, 345 (1995).

[55] F. Festy, A. Demming, and D. Richards, Ultramicroscopy **100**, 437 (2004).

[56] A. L. Demming, F. Festy, and D. Richards, J. Chem. Phys. **122**, 184716 (2005).

[57] M. Sukharev and T. Seideman, J. Phys. Chem. A **113**, 7508 (2009).

[58] S. Eisler, A. D. Slepkov, E. Elliott, T. Luu, R. McDonald, F. A. Hegmann, and R. R. Tykwinski, J. Am. Chem. Soc. **127**, 2666 (2005).

[59] R. N. Zare, Angular Momentum: Understanding Spatial Aspects in Chemistry and Physics (John Wiley & Sons, New York, NY, USA, 1988).

[60] L. Bartels, F. Wang, D. Möller, E. Knoesel, and T. F. Heinz, Science **305**, 648 (2004).

[61] M. Feng, J. Lee, J. Zhao, J. T. Yates Jr, and H. Petek, J. Am. Chem. Soc. **129**, 12394 (2007).

[62] R. W. Carpick, D. Y. Sasaki, M. S. Marcus, M. A. Eriksson, and A. R. Burns, J. Phys.: Condens. Matter **16**, R679 (2004).

[63] J. S. Hovis, H. Liu, and R. J. Hamers, Surf. Sci. **402-404**, 1 (1998).

[64] S. N. Patitsas, G. P. Lopinski, O. Hul'ko, D. J. Moffatt, and R. A. Wolkow, Surf. Sci. **457**, L425 (2000).

[65] S. Alavi, R. Rousseau, and T. Seideman, J. Chem. Phys. **113**, 4412 (2000).

[66] The adsorption potentials for the large and small clusters disagreed with each other near the surface ($\theta \rightarrow 90^{\circ}$) since the small cluster did not have the necessary silicon and hydrogen atoms to sterically repel the molecule. This region of angular parameter space is not visited in our simulations.

[67] Y. Shao, L. F. Molnar, Y. Jung, J. Kussmann, C. Ochsenfeld, S. T. Brown, A. T. B. Gilbert, L. V. Slipchenko, S. V. Levchenko, D. P. O'Neill, R. A. DiStasio Jr, R. C. Lochan, T. Wang, G. J. O. Beran, N. A. Besley, J. M. Herbert, C. Yeh Lin, T. Van Voorhis, S. Hung Chien, A. Sodt, R. P. Steele, V. A. Rassolov, P. E. Maslen, P. P. Korambath, R. D. Adamson, B. Austin, J. Baker, E. F. C. Byrd, H. Dachsel, R. J. Doerksen, A. Dreuw, B. D. Dunietz, A. D. Dutoi, T. R. Furlani, S. R. Gwaltney, A. Heyden, S. Hirata, C.-P. Hsu, G. Kedziora, R. Z. Khalliulin, P. Klunzinger, A. M. Lee, M. S. Lee, W. Liang, I. Lotan, N. Nair, B. Peters, E. I. Proynov, P. A. Pieniazek, Y. Min Rhee, J. Ritchie, E. Rosta, C. D. Sherrill, A. C. Simmonett, J. E. Subotnik, H. L. Woodcock III, W. Zhang, A. T. Bell, A. K. Chakraborty, D. M. Chipman, F. J. Keil, A. Warshel, W. J. Hehre, H. F. Schaefer III, J. Kong, A. I. Krylov, P. M. W. Gill, and M. Head-Gordon, Phys. Chem. Chem. Phys. **8**, 3172 (2006).

[68] The specific choice of frequency is immaterial so long as it is both below the substrate's bandgap and far from molecular resonances since the laser field interacts with the polarizability tensor of the molecule (as modified by the substrate), which is essentially equal to its DC value at these frequencies. In fact, it can be shown that the field-matter interaction is independent of the frequency [10].

[69] M. W. Schmidt, K. K. Baldridge, J. A. Boatz, S. T. Elbert, M. S. Gordon, J. H. Jensen, S. Koseki, N. Matsunaga, K. A. Nguyen, S. J. Su, T. L. Windus, M. Dupuis, and J. A. Montgomery, J. Comput. Chem. **14**, 1347 (1993).

[70] A. Taflove and S. C. Hagness, Computational Electrodynamics: The Finite-Difference Time-Domain Approach 3rd ed. (Artech House, Boston, MA, USA, 2005).

[71] http://code.google.com/p/m-a-d-n-e-s-s/.

[72] J. M. McMahon, S. K. Gray, and G. C. Schatz, Nano Lett. **10**, 3473 (2010).

[73] M. G. Reuter, J. C. Hill, and R. J. Harrison, Comput. Phys. Commun. **183**, 1 (2012).

[74] K. Blum, Density Matrix Theory and Applications, 3rd ed. (Springer-Verlag, Heidelberg, Germany, 2012).

[75] M. D. Feit, J. A. Fleck Jr, and A. Steiger, J. Comput. Phys. **47**, 412 (1982).

[76] M. D. Feit and J. A. Fleck Jr, J. Chem. Phys. **78**, 301 (1983).

[77] M. R. Hermann and J. A. Fleck Jr, Phys. Rev. A **38**, 6000 (1988).

[78] M. G. Reuter, M. A. Ratner, and T. Seideman, J. Chem. Phys. **131**, 094108 (2009).

[79] F. W. J. Olver, D. W. Lozier, R. F. Boisvert, and C. W. Clark, eds., NIST Handbook of Mathematical Functions (Cambridge University Press, Cambridge, UK, 2010).

[80] M. Tygert, J. Comput. Phys. **227**, 4260 (2008).

[81] M. Tygert, J. Comput. Phys. **229**, 6181 (2010).

[82] R. Kosloff, J. Phys. Chem. **92**, 2087 (1988).

[83] T. V. Basova, V. G. Kiselev, V. A. Plyashkevich, P. B. Cheblakov, F. Latteyer, H. Peisert, and T. Chassè, Chem. Phys. **380**, 40 (2011).

[84] H. Kim, S. S. Jang, R. A. Kiehl, and W. A. Goddard, J. Phys. Chem. C **115**, 3722 (2011).

[85] G.-Q. Li, M. Schreiber, and U. Kleinekathöfer, Europhys. Lett. **79**, 27006 (2007).

[86] P. Banerjee, D. Conklin, S. Nanayakkara, T.-H. Park, M. J. Therien, and D. A. Bonnell, ACS Nano **4**, 1019 (2010).